

1 **Summer-Winter Contrast in the Response of**
2 **Precipitation Extremes to Climate Change over**
3 **Northern Hemisphere Land**

4 **Andrew I. L. Williams¹ and Paul A. O’Gorman²**

5 ¹Atmospheric, Oceanic and Planetary Physics, Department of Physics, University of Oxford, Oxford, UK,
6 ²Department of Earth, Atmospheric and Planetary Sciences, Massachusetts Institute of Technology,
7 Cambridge, MA, USA

8 **Key Points:**

- 9 • Over Northern Hemisphere extratropical land, the projected fractional increase
10 of precipitation extremes is weaker in summer than winter
11 • The summer-winter contrast is mostly driven by weakened extreme ascent in sum-
12 mer, which is correlated with decreased surface relative humidity
13 • The summer-winter contrast is also evident in observations of historical changes
14 in daily precipitation extremes, consistent with CMIP5 models

Abstract

Climate models project a distinct seasonality to future changes in daily extreme precipitation. In particular, models project that over land in the extratropical Northern Hemisphere the summer response is substantially weaker than the winter response in percentage terms. Here we decompose the projected response into thermodynamic and dynamic contributions and show that the seasonal contrast arises due to a negative dynamic contribution in northern summer, and a positive dynamic contribution and an anomalously strong thermodynamic contribution in northern winter. The negative dynamic contribution in northern summer is due to weakened ascent and is strongly correlated with decreases in mean near-surface relative humidity which tend to inhibit convection. Finally, we show that the summer-winter contrast is also evident in observed trends of daily precipitation extremes in northern midlatitudes, which provides support for the contrast found in climate-model simulations.

Plain Language Summary

Extreme rainfall is a highly impactful aspect of the water cycle, and it is now well-established that global warming tends to increase the severity of extreme rainfall events. However, while this increase holds robustly on global scales, there is significant uncertainty associated with understanding the response of extreme rainfall to warming in different regions of the world and in different seasons. Here we focus on understanding changes in extreme rainfall in summer and winter over Northern Hemisphere extratropical land. We find that global warming has a contrasting impact on extreme rainfall over this region depending on the season considered. In winter, there are large increases in extreme rainfall with warming relative to the climatology, whereas in summer the changes are much weaker. We use a simple, physics-based approach to decompose these changes into contributions from changes in temperature and changes in ascent. Our results show that the contrasting seasonal response over this region is mostly due to decreases in extreme ascent with warming in summer, and that the ‘summer-winter’ contrast is already present in observed changes of extreme rainfall since the mid-20th century.

1 Introduction

The impacts of extreme precipitation are felt acutely across the world with consequences ranging from floods and landslides (Kirschbaum et al., 2012) to changes in ecosystems (Knapp et al., 2008). Additionally, it is now well-understood that extreme precipitation events intensify overall on a global scale in response to global warming (Wehner et al., 2020; Kharin et al., 2013; O’Gorman, 2015). On regional scales however, the response of precipitation extremes to warming is uncertain, with some regions projected to experience changes in precipitation extremes which are much higher or lower than the global-mean intensification (Pfahl et al., 2017). Put together, this makes regional changes in extreme precipitation potentially one of the most impactful consequences of global warming. Thus, understanding historical and future changes in regional extreme precipitation important not only from a scientific perspective, but also for understanding the unequal impacts of climate change (Diffenbaugh & Burke, 2019). In addition, considering precipitation extremes in different seasons helps to clarify physical drivers and can also be important for impacts.

To understand projections of changes in precipitation extremes it is useful to decompose the changes into contributions from different physical drivers. One such approach is to use the simple, physical scaling developed by O’Gorman and Schneider (2009a) which relates the intensity of precipitation extremes, P_e , to the pressure vertical velocity (ω_e) and the vertical derivative of saturation specific humidity with respect to pressure assuming a moist adiabatic lapse rate ($\frac{dq_s}{dp}|_{\theta^*}$),

$$P_e \sim - \left\{ \omega_e \frac{dq_s}{dp} \Big|_{\theta^*} \right\}, \quad (1)$$

where $\{\cdot\}$ denotes a mass-weighted vertical integral over the troposphere, ω_e is evaluated on the day of the extreme event, and $\frac{dq_s}{dp}|_{\theta^*}$ is evaluated using the temperature T_e on the day of the extreme event. Thus, when considering a change in precipitation extremes due to global warming, δP_e , we can decompose the change into a thermodynamic contribution associated with changes in T_e and a dynamic contribution associated with changes in extreme ascent ω_e ,

$$\delta P_e \approx \delta P_{\text{thermodynamic}} + \delta P_{\text{dynamic}}. \quad (2)$$

64 Pfahl et al. (2017) recently showed that Eq. 1 successfully captures the present-
 65 day and future changes of precipitation extremes in simulations from the Coupled Model
 66 Intercomparison Project Phase 5, CMIP5, (Taylor et al., 2012) and thus is a good proxy
 67 for understanding and decomposing these future changes (Fig. S1). Pfahl et al. (2017)
 68 used Eq. 1 to decompose future regional changes in annual and seasonal maximum daily
 69 precipitation (hereafter, Rx1day) in the CMIP5 simulations into thermodynamic and dy-
 70 namic contributions. The thermodynamic contribution is positive and relatively spatially
 71 uniform, whereas the dynamic contribution varies strongly between regions and seasons
 72 and can either locally amplify or counteract the increases from the thermodynamic con-
 73 tribution.

74 The results of Pfahl et al. (2017) show a pronounced ‘summer-winter’ contrast in
 75 the response of seasonal Rx1day. The fraction of Northern Hemisphere (NH) extratrop-
 76 ical land experiencing robust increases is relatively small in June-July-August (JJA), due
 77 to a negative dynamic contribution over land, particularly over Europe and North Amer-
 78 ica. Similar results were found by Tandon et al. (2018) for the CanESM2 large ensem-
 79 ble. By contrast, Pfahl et al. (2017) found a strong response of precipitation extremes
 80 in the NH extratropics for December-January-February (DJF), and climate change was
 81 found to induce a shift in precipitation extremes towards the cold season in this region.
 82 Marelle et al. (2018) also found a shift towards the cold season for many regions in both
 83 CMIP5 models and regional models from the Coordinated Regional Downscaling Exper-
 84 iment (CORDEX). Furthermore, Marelle et al. (2018) found that the CMIP5 and CORDEX
 85 models reproduce most aspects of the seasonality of precipitation extremes in the cur-
 86 rent climate when compared to gridded observations, which increases confidence in their
 87 future projections for changes in seasonality.

88 High-resolution, regional models have also shown a weaker response of precipita-
 89 tion extremes to climate change in JJA than DJF in Europe (Wood & Ludwig, 2020).
 90 This summer-winter contrast was also found in convection-permitting simulations of the
 91 Mediterranean (Pichelli et al., 2021) and the Contiguous United States (Prein et al., 2017),
 92 which is notable since convection-permitting simulations are better able to represent short-
 93 duration precipitation extremes (Prein et al., 2015). Precipitation extremes in JJA are
 94 known to be sensitive to how convection is represented (Chan et al., 2014; Prein et al.,
 95 2015; Ban et al., 2015; Kooperman et al., 2014), and caution is needed for projections
 96 in regions and seasons with significant mesoscale convective activity, particularly for sub-
 97 daily extremes. This emphasizes the importance of seeking observational evidence and
 98 robust physical mechanisms that may support projected seasonal changes in precipita-
 99 tion extremes.

100 Here, we focus on the summer-winter contrast in the fractional response of daily
 101 precipitation extremes to climate warming in the NH in CMIP5 models and gridded ob-
 102 servations. We begin by describing the model output and observational data and the meth-
 103 ods of analysis (Section 2). We then show that the JJA-DJF contrast is primarily due
 104 to differences in the dynamic contribution between JJA and DJF, but that differences

105 in the thermodynamic contribution also play a role, particularly at high latitudes (Sec-
106 tion 3). We further show that the negative dynamic contribution in JJA is strongly cor-
107 related in terms of model scatter and spatial pattern to decreases in mean near-surface
108 relative humidity over land, suggesting a possible mechanism through a less favorable
109 convective environment (Section 4). Finally, we demonstrate that the summer-winter con-
110 trast is also evident in gridded observational datasets and CMIP5 simulations over the
111 historical period (Section 5), before giving our conclusions (Section 6).

112 2 Methods

113 We analyse changes over 1950–2100 under the historical and RCP8.5 scenarios for
114 CMIP5. All models are used that provide the required data (listed in Text S1). The scal-
115 ing and decomposition based on Eq. 1 is taken from Pfahl et al. (2017), and further de-
116 tails can be found there, but we repeat the key points of the calculation here. We chose
117 not to repeat their calculations with CMIP6 output because there is little improvement
118 in the simulation of daily precipitation extremes between CMIP5 and CMIP6 (Wehner
119 et al., 2020).

120 Daily surface precipitation was used to calculate the maximum daily precipitation
121 amount (Rx1day) for JJA and DJF in each year. Daily-mean temperature and vertical
122 pressure velocity on all available pressure levels at the location and day of each daily-
123 maximum precipitation event (T_e and ω_e , respectively) were then used to calculate the
124 full extreme precipitation scaling following Eq. 1 by performing a vertical integral over
125 all tropospheric levels with ascent ($\omega_e < 0$). To calculate the thermodynamic contri-
126 bution, this analysis is repeated but with ω_e replaced with its average over all years from
127 1950-2100.

128 To calculate the sensitivity to climate change, we first normalize Rx1day and the
129 full and thermodynamic scalings by dividing by their average over the historical period
130 (1950-2000). We then calculate the dynamic contribution as the difference between the
131 full and thermodynamic scaling. This approach to calculating the dynamic contribution
132 differs slightly from Pfahl et al. (2017), but yields similar results (e.g., compare our Fig.
133 1c with their Fig. S8d). We then regress these normalized time series against global- and
134 annual-mean surface temperature anomalies over 1950-2000 using the Theil-Sen estima-
135 tor to produce sensitivities in units of (% K⁻¹). The Theil-Sen estimator is a non-parametric
136 estimator which operates by choosing the median of the slopes of all lines through pairs
137 of points and is less sensitive to outliers than ordinary least-squares regression. This re-
138 gression approach has been shown to provide more robust results compared to taking
139 differences in multi-decadal means (Fischer et al., 2014). When presenting results for the
140 seasonal contrast (JJA-DJF), the sensitivities are calculated by differencing the normal-
141 ized JJA and DJF time series in each grid box, before regressing this ‘difference’ time
142 series against global-mean surface temperature anomalies for each model. Using a nor-
143 malization over a reference period can sometimes produce statistical biases for changes
144 in precipitation extremes (Donat et al., 2016; Sippel et al., 2017), but our results remain
145 largely unchanged when using the full 1950-2100 period for normalization (Fig. S2).

146 All analysis is performed on each model’s native grid, and then the sensitivities are
147 re-gridded to a uniform 1°x1° grid before calculating multi-model statistics and zonal
148 means. Pfahl et al. (2017) noted previously that some models produce very low seasonal
149 Rx1day at some grid points in the subtropics, which creates anomalously large extreme
150 precipitation sensitivities. Thus, when calculating multi-model or zonal means we ex-
151 clude grid boxes from models where the average seasonal Rx1day over the historical pe-
152 riod is less than 0.5 mm day⁻¹. Additionally, we found that the CMCC-CMS model pro-
153 duced unrealistically large changes in the thermodynamic contribution over Pakistan and
154 Afghanistan, and so for this model we exclude the region from 29.5° to 32.5° latitude
155 and 60° to 68° longitude.

We also analyse changes in seasonal Rx1day over the historical period over land in observations and compare them to the same period in the CMIP5 simulations (combining the historical and RCP8.5 simulations). We analyse the ‘extended’ NH summer (MJJAS) and winter (NDJFM) seasons (as opposed to JJA and DJF) to improve the signal-to-noise ratio and use data from 1950-2017, with the time-period chosen for maximum overlap with the CMIP5 data. For Rx1day observations, we focus on the HadEX3 gridded dataset (Dunn et al., 2020) which has a spatial resolution of $1.25^\circ \times 1.875^\circ$, but we also show results for the GHCNDEX observational dataset over 1952-2018 (Donat et al., 2013) which has a resolution of $2.5^\circ \times 2.5^\circ$ in the supplement as a point of comparison. To calculate annual- and global-mean surface temperatures (including land and ocean) from observations, we use the NOAA Merged Land-Ocean Surface Temperature Analysis (Vose et al., 2012).

Sensitivities in $\% K^{-1}$ for the observations are calculated at each gridbox as described earlier but requiring at least 45 years of data at that grid box and normalizing by an average over all the years used. When analysing the summer-winter contrast (here, MJJAS-NDJFM) we require each grid box to have 45 years of data for both seasons in each year, and we normalize each time series separately before differencing and then performing the regression. CMIP5 data are subsampled to the observations in both space and time. To reduce the influence of unforced variability and outliers, we then aggregate the sensitivities into 5° latitude bands and calculate the median sensitivity across each latitude band. We use bootstrapping to estimate the uncertainty due to inter-annual variability and the non-uniform spatial coverage of the observations. To do this we calculate 10,000 bootstrap samples per latitude band, where each sample involves a random choice of both the years used for each grid box to calculate the regression, and a random choice of the grid boxes used to calculate the median sensitivity across the latitude band. We then calculate the median sensitivity for each bootstrap sample, and then the 90% confidence interval across samples for each latitude band. Our conclusions are largely insensitive to the size of the latitude bands and the number of bootstrap samples used, except in the tropics where larger latitude bands can obscure seasonal migrations of the ITCZ.

3 Summer-Winter contrast in CMIP5

Figure 1 shows the multi-model mean patterns of seasonal Rx1day sensitivity based on the scaling Eq. 1 and its decomposition into thermodynamic and dynamic contributions for JJA, DJF and JJA-DJF. As found in previous studies, the thermodynamic contribution is relatively uniform with robust agreement on the sign and the magnitude in both seasons. In stark contrast, the dynamic contribution exhibits strong regional and seasonal variations.

The NH extratropics show a strongly negative JJA-DJF contrast especially over land (Fig. 1g). Over this region, the DJF response (Fig. 1d) is amplified by a positive contribution from the dynamics (Fig. 1f) and a relatively strong thermodynamic contribution particularly at high latitudes (Fig. 1e). On the other hand, the response during JJA is ‘muted’, with much less multi-model agreement and with some regions (particularly Europe and the continental United States) exhibiting close to no change or even negative responses of extreme precipitation to warming (Fig. 1a). This weak JJA response arises predominantly due to the strongly negative dynamic contribution (Fig. 1c) which cancels out the robust, positive increase due to the thermodynamic contribution (Fig. 1b). The negative dynamic contribution in JJA is particularly strong over land and parts of the subtropical Atlantic. A land-ocean contrast in the dynamic contribution in JJA is apparent when examining anomalies from the zonal-mean (Fig. S3), which show that the negative dynamic contribution extends further poleward over NH land as compared to ocean. The combination of the very weak response in JJA and the amplified response in DJF leads to the strong JJA-DJF difference in the response, particularly over NH mid-

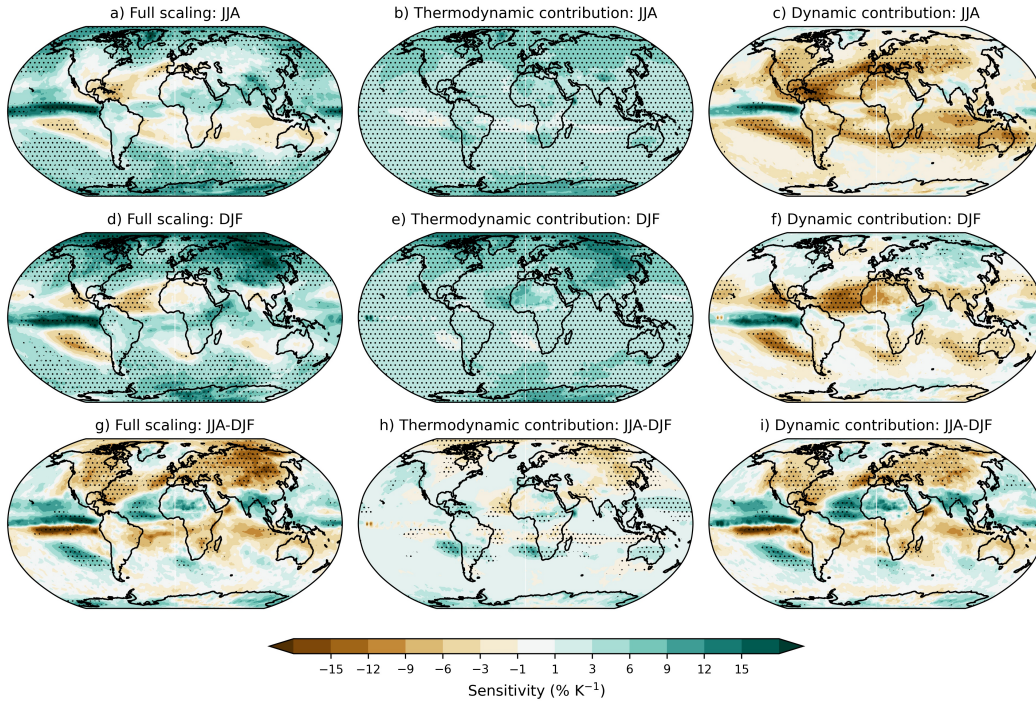


Figure 1. Multi-model mean Rx1day sensitivity over 1950-2100 according to the scaling Eq. 1 (a,d,g) and decomposition into (b,e,h) thermodynamic and (c,f,i) dynamic contributions for (a-c) JJA, (d-f) DJF and (e-i) JJA minus DJF, the summer-winter contrast. Stippling indicates where at least 90% of the models agree on the sign of the change.

208 latitude land. The dynamic contribution is responsible for most of the JJA-DJF differ-
 209 ence, as illustrated by the similarity between Fig. 1g and i, but seasonal differences in
 210 the thermodynamic contribution also play a role (Fig. 1h).

211 We next examine zonal-mean changes in the scaling decomposition over both land and
 212 ocean and over land only (Fig. 2). The thermodynamic contribution is larger at higher
 213 latitudes (e.g., Fig. 2b,e) and is partly responsible for the JJA-DJF contrast at NH
 214 middle and high latitudes (Fig. 2c,f), implying a stronger thermodynamic contribution in
 215 DJF than JJA. A stronger thermodynamic contribution is expected for the lower tem-
 216 peratures in winter and at higher latitudes because percentage increases in $\frac{dq_{\pm}}{dp}|_{\theta^*}$ with
 217 increasing temperature are larger at lower temperatures (O’Gorman & Schneider, 2009a).
 218 It could also be argued that Arctic amplification of surface warming also plays a role,
 219 and indeed the JJA-DJF contrast in the NH thermodynamic contribution is negligible
 220 when we regress against zonal-mean temperature (Fig. S4). However, the stronger ther-
 221 modynamic contribution at higher (and colder) latitudes is also found to occur even when
 222 a globally uniform surface warming is imposed (O’Gorman et al., 2021) suggesting that
 223 it is not tied to Arctic amplification. Additionally, previous studies have found there is
 224 less warming of T_e than mean temperature at middle and high latitudes (e.g., Fig. S5
 225 of O’Gorman and Schneider (2009a) or Fig. 8c of O’Gorman and Schneider (2009b)) which
 226 suggests that normalizing by the local changes in zonal-mean temperature gives too much
 227 emphasis to Arctic amplification.

228 In the tropics, the zonal-mean results in Fig. 2 are consistent with amplification
 229 of precipitation extremes along the ITCZ region, which moves seasonally. This leads to
 230 a southward shift in precipitation extremes when considering the summer-winter con-

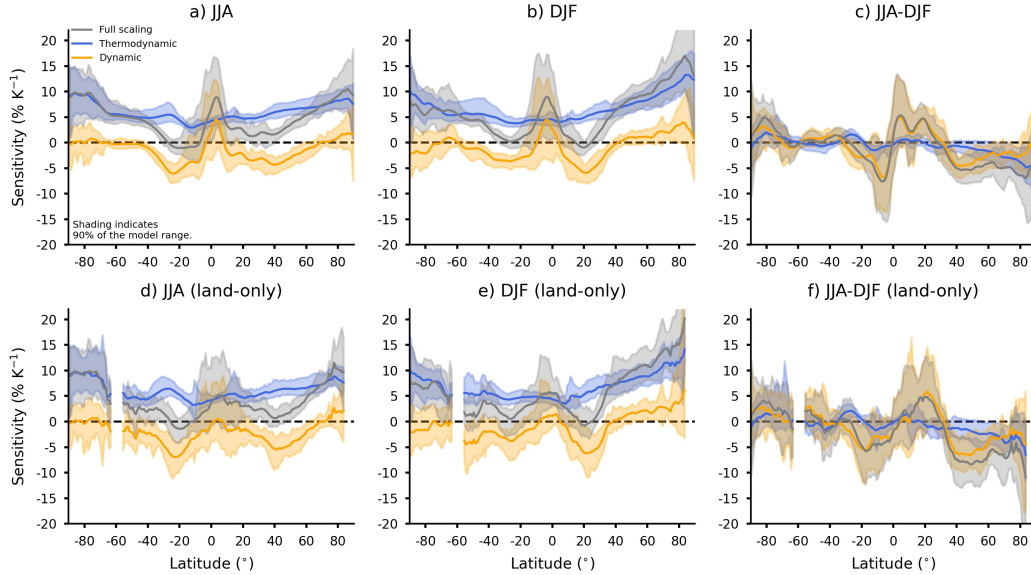


Figure 2. Zonal-mean of the Rx1day sensitivity over 1950-2100 according to the scaling and its decomposition into thermodynamic and dynamic contributions for (a) JJA, (b) DJF and (c) JJA-DJF. Lines indicate multi-model means and shading shows the 90% model range. Panels (d,e,f) show the same results but for over land only.

231 trast (Fig. 2c,f) because the ITCZ occurs further south in DJF than in JJA. These shifts
 232 are driven by the dynamic contribution as demonstrated by the similarity between the
 233 changes in the full scaling and the dynamic contribution in the tropics (gray and orange
 234 lines in Fig. 2c,f).

235 We have presented results in terms of percentage changes in ($\% \text{ K}^{-1}$) as opposed
 236 to absolute changes ($\text{mm day}^{-1} \text{ K}^{-1}$) because it is useful to consider the change in each
 237 season relative to what is expected for that season and because previous studies have also
 238 focused on percentage changes which are easier to relate to physical processes. Absolute
 239 changes also show a seasonal contrast for much of NH midlatitude land but not for some
 240 parts of Asia (Fig. S5g) or for zonal-mean quantities (Fig. S6f), because the thermody-
 241 namic contribution offsets the dynamic contribution when considering absolute changes.
 242 Thus, one additional advantage of considering percentage changes is that it provides a
 243 strong zonal-mean signal to look for in the observational record (Section 5).

244 4 Physical mechanisms of the negative dynamic contribution in JJA

245 Dynamic weakening of precipitation extremes during JJA is a large contributor to
 246 the JJA-DJF contrast in the extratropical NH, particularly over land (Figs. 1c and 2d).
 247 Physically then, what mechanisms could be responsible for this dynamic weakening? Tandon
 248 et al. (2018) tackled this question using a three-term approximation of the QG- ω equa-
 249 tion and found the weakening of extreme ascent was related to increases in the horizon-
 250 tal length scale of extreme ascent. However, Li and O’Gorman (2020) numerically in-
 251 verted the QG- ω equation in extreme precipitation events and found that changes in eddy
 252 length were less important when all terms were retained in the QG- ω equation, although
 253 they did not separately analyse extremes in JJA. Changes in moist static stability, σ_m ,
 254 have also been found to be important in previous studies (Li & O’Gorman, 2020; Tan-
 255 don et al., 2018), with an increase in σ_m associated with a weakening of ascent. Here,

256 we calculate changes in moist static stability on the days of the extreme events follow-
 257 ing previous work (Text S2) and find that the changes in moist static stability are mostly
 258 consistent with the spatial pattern of the JJA dynamic contribution (Fig. S7), but they
 259 fail to capture the inter-model spread in projections over NH land (Fig. S8).

260 We next investigate an alternative explanation for the dynamic contribution over
 261 NH extratropical land in JJA in terms of changes in the near-surface relative humidity
 262 (RH_{2m}). Decreases in RH_{2m} over land are expected with global-warming because of the
 263 land-ocean warming contrast (Byrne & O’Gorman, 2016, 2018) and decreases in stom-
 264 atal conductance (Cao et al., 2010; Berg et al., 2016). Furthermore, previous work has
 265 already shown that decreases in relative humidity cause an increase in convective inhibi-
 266 tion (CIN) that is particularly large over NH land in JJA (Chen et al., 2020).

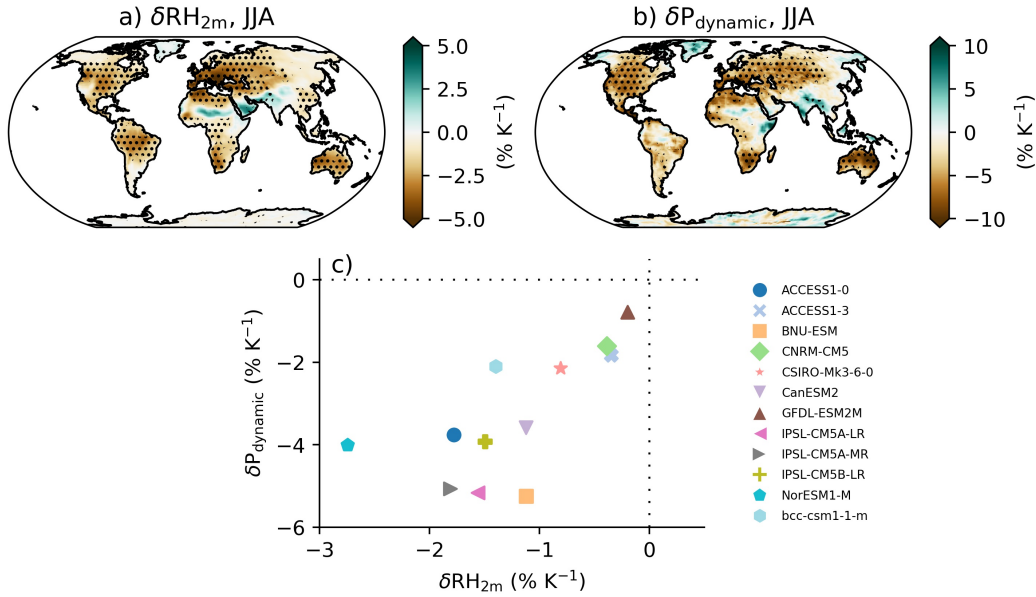


Figure 3. Sensitivity for JJA over 1950-2100 of (a) seasonal-mean near-surface relative humidity and (b) the dynamic contribution to changes in precipitation extremes. Results are shown for the 12 models that archived RH_{2m} and for which the dynamic contribution was calculated. Stippling indicates where 10 out of the 12 models agree on the sign of the sensitivity. Panel (c) shows a scatter plot of the median sensitivities across land grid boxes in the latitude band 40-70°N for each model.

267 In Fig. 3 we compare the sensitivities of seasonal-mean RH_{2m} and the dynamic contribu-
 268 tion to precipitation extremes during JJA for climate change over 1950-2100. The
 269 sensitivity of RH_{2m} is defined using regression analogously to the sensitivity of precipi-
 270 tation extremes and normalized by the 1950-2000 mean. There is strong agreement
 271 between the spatial pattern of the change in RH_{2m} and the dynamic contribution (Fig. 3a,b),
 272 with the models agreeing robustly on strong decreases in relative humidity and a nega-
 273 tive dynamic contribution over similar regions of the globe. Furthermore, Fig. 3c shows
 274 that models with a stronger decrease in JJA RH_{2m} also tend to have a stronger nega-
 275 tive dynamic contribution when averaged over NH midlatitude land. This suggests a mech-
 276 anism whereby decreases in RH_{2m} over NH land during JJA lead to a less-favorable en-
 277 vironment for the convective heating that amplifies ascent in precipitation extremes. The
 278 link between the dynamic contribution and RH_{2m} is not as strong in individual model
 279 runs (Fig. S9 and S10), potentially due to unforced variability in precipitation extremes

and other mechanisms which act to change ω_e in precipitation extremes but are not robust across models. Changes in $\text{RH}_{2\text{m}}$ on the day of the event are weaker but are nonetheless strongly correlated with the dynamic contribution (Fig. S11).

The details of the mechanism by which decreases in relative humidity inhibit convective heating in extreme precipitation events requires further study, ideally with a cloud-resolving model. One possibility is through increases in seasonal-mean CIN, which we find are correlated with the dynamic contribution for both the spatial pattern and inter-model scatter (Text S3, Fig. S12). CIN on the day of the extreme precipitation event also increases, but the correlation with the dynamic contribution is weaker (see Figs. S13-14 and discussion in Text S3). Another possibility is that decreases in relative humidity inhibit convective heating through entrainment of relatively drier environmental air, and this is plausible because the region of decreased relative humidity over land extends upwards through the lower troposphere (Chen et al., 2020).

The relationship between changes in mean relative humidity and the negative dynamic contribution to changes in extreme precipitation in JJA (Fig. 3) is notable in that it links changes in a mean quantity to changes in an extreme statistic. Such a link is potentially very useful since mean quantities can be easier to observationally constrain than extremes. The decrease in relative humidity occurs only over land, and factors such as a general weakening of the extratropical storm track in NH JJA (O’Gorman, 2010; Gertler & O’Gorman, 2019), poleward expansion of the Hadley cells in the subtropics (Pfahl et al., 2017; Norris et al., 2020), or other aspects of the large-scale dynamics (Tandon et al., 2018) may also influence the dynamic contribution over land and ocean.

In NH DJF, there is not a connection between changes in $\text{RH}_{2\text{m}}$ and the dynamic contribution (Fig. S15), which we hypothesize is because daily precipitation extremes in DJF are controlled to a greater extent by large-scale dynamics as compared to the strongly convective extremes in JJA.

Interestingly, there is also a negative dynamic contribution over the Southern Hemisphere over both land and ocean in JJA (Fig. 1c). This negative dynamic contribution does not show as clear a land-ocean contrast and primarily occurs at lower latitudes as compared to the negative dynamic contribution in the NH, and thus we hypothesize it may be more strongly influenced by factors such as Hadley cell expansion (Pfahl et al., 2017; Norris et al., 2020).

5 Observed and modelled trends over the historical period

Given the difficulty in correctly representing convection in models, we next turn our attention to gridded observations of precipitation extremes. Figure 4 shows the sensitivity of daily precipitation extremes from HadEX3 observations and CMIP5 models to warming over 1950-2017 for boreal summer (MJJAS) and extended winter (NDJFM), and the seasonal contrast (MJJAS-NDJFM). The results are expressed as medians for each 5° latitude bands (see Section 2). For the NH extratropics, the observed sensitivities are positive in both MJJAS and NDJFM, and there is a clear summer-winter contrast with lower sensitivities in MJJAS than NDJFM (Fig.4a,b,c). The seasonal contrast is also evident when looking at maps of the sensitivities, but as expected there is considerable noise when considering sensitivities for a period of this length in individual grid-boxes (Fig.S16 a,b,c). The NH extratropical summer-winter contrast is also present in the CMIP5 models over the same historical period (Fig.4 d,e,f).

We next quantify the NH midlatitude response by averaging the sensitivities over land between $30\text{-}70^\circ\text{N}$ with area-weighting. For the observations, the mean NH sensitivity is $5.6\% \text{ K}^{-1}$ for MJJAS, $11.6\% \text{ K}^{-1}$ for NDJFM, and $-7.2\% \text{ K}^{-1}$ for MJJAS-NDJFM. For the CMIP5 models over the same period, the multimodel-mean sensitivity and full model range are $4.4\% \text{ K}^{-1}$ (2.1 to $9.1\% \text{ K}^{-1}$) for MJJAS, $7.0\% \text{ K}^{-1}$ (4.7

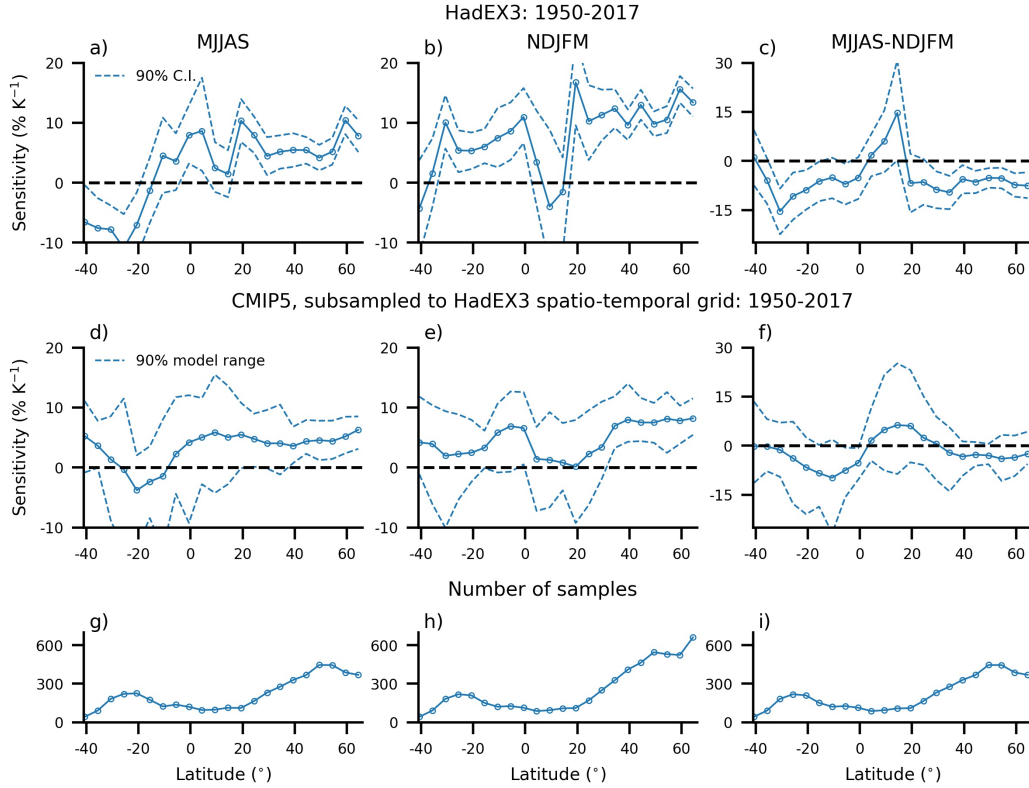


Figure 4. The sensitivity of Rx1day to warming over 1950-2017 in MJJAS (a,d), NDJFM (b,e) and MJJAS-NDJFM (c,f) for the HadEX3 dataset (a,b,c) and CMIP5 simulations subsampled to the HadEX3 dataset (d,e,f). Solid lines show the median sensitivity across the 5° latitude band. Dashed lines show the 90% confidence interval for HadEX3 and 90% of the model spread for CMIP5. The total number of samples included in each latitude band is also shown (g,h,i) which is the same for both the observations and the simulations.

330 to 10.8 % K⁻¹) for NDJFM, and -2.4 % K⁻¹ (0.6 to -8.4 % K⁻¹) for MJJAS-NDJFM.
 331 Thus, while the models and observations show similar sensitivities during MJJAS, none
 332 of the models capture the very strong observed sensitivity for NDJFM. As a result, while
 333 the observed MJJAS-NDJFM contrast lies within the model range, the multi model-mean
 334 value is smaller in magnitude than the value in observations. The smaller magnitude of
 335 the sensitivity in the multimodel mean than in observations may be related to unforced
 336 internal variability, which is reduced by considering the multimodel mean but is likely
 337 to be still important in observations. Despite this, most but not all models (15/18) give
 338 a negative MJJAS-NDJFM contrast for this period, consistent with the observations.

339 GHCNDEX has a coarser spatial resolution and fewer grid boxes with data compared to
 340 HadEX3, particularly in the tropics, but we find similar changes in seasonal Rx1day
 341 over the Northern Hemisphere (Figs. S16 and S17), which strengthens our confidence
 342 in the results. Similar results are also found when the CMIP5 data are not subsampled
 343 to the observations (Figure S18), which suggests that missing grid points in the obser-
 344 vations are not affecting our conclusions. The robust presence of the MJJAS-NDJFM
 345 contrast in observed trends over the historical period supports the contrast found in ear-
 346 lier sections.

6 Conclusions

In this study we have demonstrated that CMIP5 models project a robust summer-winter contrast in the response of precipitation extremes to warming over Northern Hemisphere midlatitude land, with considerably weaker percentage changes in JJA than DJF. We have also shown that this summer-winter contrast is evident in gridded observations over the historical period, which strengthens our confidence in the future projections. CMIP5 simulations over the historical period also show a summer-winter contrast that occurs in 15/18 models, and the model range includes the observed value of this contrast.

Furthermore, we have used a simple, physical scaling to help explain the cause of the summer-winter contrast in changes in precipitation extremes. The contrast is primarily caused by the dynamic contribution (related to changes in extreme ascent) with strongly negative dynamic contribution in JJA and a weakly positive dynamic contribution in DJF. The negative dynamic contribution in JJA is strong over NH extratropical land, and we show it is highly correlated with decreases in near-surface relative humidity and increases in convective inhibition in terms of spatial pattern and inter-model scatter, suggesting a potential mechanism whereby reduced relative humidity during JJA provides a less favorable environment for strong convective heating and ascent.

The thermodynamic contribution to changes in precipitation extremes also helps to amplify the response in winter over summer, particularly over high latitudes. We have focused on percentage seasonal changes because they may be more relevant for impacts in a given season and to better connect with physical mechanisms. If absolute rather than percentage changes in precipitation extremes are considered, the thermodynamic contribution is larger in summer than winter, and this offsets the JJA-DJF contrast in the dynamic contribution, although the contrast is still evident over much of NH midlatitude land (Fig. S5).

Future work could build on our observational analysis by performing a formal detection and attribution analysis of the seasonal difference in trends of precipitation extremes. Future work could also build more understanding of the positive dynamic contribution in the NH extratropics in winter, which is important as DJF is the season of maximum daily precipitation in many regions (Marelle et al., 2018). Future work could also investigate the detailed mechanism (e.g., involving CIN or convective entrainment) and physical accuracy of the link between changes in relative humidity and precipitation extremes in summer using idealized experiments in cloud-resolving models. Given the potential importance of decreases in relative humidity over land for convection and precipitation extremes, it would be helpful to develop an emergent constraint for the magnitude of the expected decrease, although this may be difficult to the extent that it depends both on the land-ocean warming contrast and the plant physiological response to increased on CO₂ levels.

7 Open Research

Processed observational and climate model data supporting the conclusions in this study can be found at <https://doi.org/10.5281/zenodo.6341493>.

Acknowledgments

A.I.L.W. acknowledges funding from the Natural Environment Research Council, Oxford DTP, award NE/S007474/1 and the Laidlaw Research and Leadership Programme. P.A.O'.G. acknowledges support from NSF awards AGS-1552195 and AGS-1749986.

We acknowledge the World Climate Research Programme's Working Group on Coupled Modelling, which is responsible for CMIP, and we thank the climate modeling groups

394 for producing and making available their model output. We thank Stephan Pfahl for gen-
 395 erously providing the CMIP5 scaling data used for this study and Ziwei Li for helpful
 396 discussions. A.I.L.W. thanks Makayla Haussler for moral support and input on the fig-
 397 ures.

398 References

- 399 Ban, N., Schmidli, J., & Schär, C. (2015). Heavy precipitation in a changing cli-
 400 mate: Does short-term summer precipitation increase faster? *Geophysical Re-*
 401 *search Letters*, *42*(4), 1165–1172. doi: 10.1002/2014GL062588
- 402 Berg, A., Findell, K., Lintner, B., Giannini, A., Seneviratne, S. I., van den Hurk, B.,
 403 ... Milly, P. C. D. (2016). Land–atmosphere feedbacks amplify aridity increase
 404 over land under global warming. *Nature Climate Change*, *6*(9), 869–874. doi:
 405 10.1038/nclimate3029
- 406 Byrne, M. P., & O’Gorman, P. A. (2016). Understanding decreases in land relative
 407 humidity with global warming: Conceptual model and GCM simulations. *Jour-*
 408 *nal of Climate*, *29*(24), 9045–9061. doi: 10.1175/JCLI-D-16-0351.1
- 409 Byrne, M. P., & O’Gorman, P. A. (2018). Trends in continental temperature
 410 and humidity directly linked to ocean warming. *Proceedings of the National*
 411 *Academy of Sciences*, *115*(19), 4863–4868. doi: 10.1073/pnas.1722312115
- 412 Cao, L., Bala, G., Caldeira, K., Nemani, R., & Ban-Weiss, G. (2010). Importance
 413 of carbon dioxide physiological forcing to future climate change. *Proceedings*
 414 *of the National Academy of Sciences*, *107*(21), 9513–9518. doi: 10.1073/pnas
 415 .0913000107
- 416 Chan, S. C., Kendon, E. J., Fowler, H. J., Blenkinsop, S., Roberts, N. M., & Ferro,
 417 C. A. T. (2014). The value of high-resolution met office regional climate mod-
 418 els in the simulation of multihourly precipitation extremes. *Journal of Climate*,
 419 *27*(16), 6155–6174. doi: 10.1175/JCLI-D-13-00723.1
- 420 Chen, J., Dai, A., Zhang, Y., & Rasmussen, K. L. (2020). Changes in convective
 421 available potential energy and convective inhibition under global warming.
 422 *Journal of Climate*, *33*(6), 2025–2050. doi: 10.1175/JCLI-D-19-0461.1
- 423 Diffenbaugh, N. S., & Burke, M. (2019). Global warming has increased global eco-
 424 nomic inequality. *Proceedings of the National Academy of Sciences*, *116*(20),
 425 9808–9813. doi: 10.1073/pnas.1816020116
- 426 Donat, M. G., Alexander, L. V., Yang, H., Durre, I., Vose, R., Dunn, R. J. H., ...
 427 Kitching, S. (2013). Updated analyses of temperature and precipitation
 428 extreme indices since the beginning of the twentieth century: The HadEX2
 429 dataset. *Journal of Geophysical Research: Atmospheres*, *118*(5), 2098–2118.
 430 doi: 10.1002/jgrd.50150
- 431 Donat, M. G., Lowry, A. L., Alexander, L. V., O’Gorman, P. A., & Maher, N.
 432 (2016). More extreme precipitation in the world’s dry and wet regions. *Nature*
 433 *Climate Change*, *6*(5), 508–513. doi: 10.1038/nclimate2941
- 434 Dunn, R. J. H., Alexander, L. V., Donat, M. G., Zhang, X., Bador, M., Herold, N.,
 435 ... Bin Hj Yussof, M. N. (2020). Development of an updated global land
 436 in situ-based data set of temperature and precipitation extremes: HadEX3.
 437 *Journal of Geophysical Research: Atmospheres*, *125*(16), e2019JD032263. doi:
 438 10.1029/2019JD032263
- 439 Fischer, E. M., Sedláček, J., Hawkins, E., & Knutti, R. (2014). Models agree on
 440 forced response pattern of precipitation and temperature extremes. *Geophysi-*
 441 *cal Research Letters*, *41*(23), 8554–8562. doi: 10.1002/2014GL062018
- 442 Gertler, C. G., & O’Gorman, P. A. (2019). Changing available energy for extra-
 443 tropical cyclones and associated convection in northern hemisphere summer.
 444 *Proceedings of the National Academy of Sciences*, *116*(10), 4105–4110. doi:
 445 10.1073/pnas.1812312116
- 446 Kharin, V. V., Zwiers, F. W., Zhang, X., & Wehner, M. (2013). Changes in tem-

- 447 perature and precipitation extremes in the CMIP5 ensemble. *Climatic Change*,
 448 *119*(2), 345–357. doi: 10.1007/s10584-013-0705-8
- 449 Kirschbaum, D., Adler, R., Adler, D., Peters-Lidard, C., & Huffman, G. (2012).
 450 Global distribution of extreme precipitation and high-impact landslides in 2010
 451 relative to previous years. *Journal of Hydrometeorology*, *13*(5), 1536–1551. doi:
 452 10.1175/JHM-D-12-02.1
- 453 Knapp, A. K., Beier, C., Briske, D. D., Classen, A. T., Luo, Y., Reichstein, M., ...
 454 Weng, E. (2008). Consequences of more extreme precipitation regimes for
 455 terrestrial ecosystems. *BioScience*, *58*(9), 811–821.
- 456 Kooperman, G. J., Pritchard, M. S., & Somerville, R. C. J. (2014). The re-
 457 sponse of US summer rainfall to quadrupled CO₂ climate change in conven-
 458 tional and superparameterized versions of the NCAR community atmosphere
 459 model. *Journal of Advances in Modeling Earth Systems*, *6*(3), 859–882. doi:
 460 10.1002/2014MS000306
- 461 Li, Z., & O’Gorman, P. A. (2020). Response of vertical velocities in extratropical
 462 precipitation extremes to climate change. *Journal of Climate*, *33*(16), 7125–
 463 7139. doi: 10.1175/JCLI-D-19-0766.1
- 464 Marelle, L., Myhre, G., Hodnebrog, , Sillmann, J., & Samset, B. H. (2018). The
 465 changing seasonality of extreme daily precipitation. *Geophysical Research Let-
 466 ters*, *45*(20), 11,352–11,360. doi: 10.1029/2018GL079567
- 467 Norris, J., Chen, G., & Li, C. (2020). Dynamic amplification of subtropical extreme
 468 precipitation in a warming climate. *Geophysical Research Letters*, *47*(14),
 469 e2020GL087200. doi: <https://doi.org/10.1029/2020GL087200>
- 470 O’Gorman, P. A., & Schneider, T. (2009a). The physical basis for increases in pre-
 471 cipitation extremes in simulations of 21st-century climate change. *Proceedings
 472 of the National Academy of Sciences*, *106*(35), 14773–14777. doi: 10.1073/pnas
 473 .0907610106
- 474 O’Gorman, P. A. (2010). Understanding the varied response of the extratropical
 475 storm tracks to climate change. *Proceedings of the National Academy of Sci-
 476 ences*, *107*(45), 19176–19180. doi: 10.1073/pnas.1011547107
- 477 O’Gorman, P. A. (2015). Precipitation extremes under climate change. *Current Cli-
 478 mate Change Reports*, *1*(2), 49–59. doi: 10.1007/s40641-015-0009-3
- 479 O’Gorman, P. A., Li, Z., Boos, W. R., & Yuval, J. (2021). Response of extreme
 480 precipitation to uniform surface warming in quasi-global aquaplanet simula-
 481 tions at high resolution. *Philosophical Transactions of the Royal Society A:
 482 Mathematical, Physical and Engineering Sciences*, *379*(2195), 20190543. doi:
 483 10.1098/rsta.2019.0543
- 484 O’Gorman, P. A., & Schneider, T. (2009b). Scaling of precipitation extremes over
 485 a wide range of climates simulated with an idealized gcm. *Journal of Climate*,
 486 *22*(21), 5676 - 5685. doi: 10.1175/2009JCLI2701.1
- 487 Pfahl, S., O’Gorman, P. A., & Fischer, E. M. (2017). Understanding the regional
 488 pattern of projected future changes in extreme precipitation. *Nature Climate
 489 Change*, *7*(6), 423–427. doi: 10.1038/nclimate3287
- 490 Pichelli, E., Coppola, E., Sobolowski, S., Ban, N., Giorgi, F., Stocchi, P., ...
 491 Vergara-Temprado, J. (2021). The first multi-model ensemble of regional
 492 climate simulations at kilometer-scale resolution part 2: historical and future
 493 simulations of precipitation. *Climate Dynamics*, *56*(11), 3581–3602. doi:
 494 10.1007/s00382-021-05657-4
- 495 Prein, A. F., Langhans, W., Fosser, G., Ferrone, A., Ban, N., Goergen, K., ... Le-
 496 ung, R. (2015). A review on regional convection-permitting climate modeling:
 497 Demonstrations, prospects, and challenges. *Reviews of Geophysics*, *53*(2),
 498 323–361. doi: 10.1002/2014RG000475
- 499 Prein, A. F., Rasmussen, R. M., Ikeda, K., Liu, C., Clark, M. P., & Holland, G. J.
 500 (2017). The future intensification of hourly precipitation extremes. *Nature
 501 Climate Change*, *7*(1), 48–52. doi: 10.1038/nclimate3168

- 502 Sippel, S., Zscheischler, J., Heimann, M., Lange, H., Mahecha, M. D., van Old-
503 enborgh, G. J., . . . Reichstein, M. (2017). Have precipitation extremes
504 and annual totals been increasing in the world’s dry regions over the last
505 60 years? *Hydrology and Earth System Sciences*, *21*(1), 441–458. doi:
506 10.5194/hess-21-441-2017
- 507 Tandon, N. F., Nie, J., & Zhang, X. (2018). Strong influence of eddy length on bo-
508 real summertime extreme precipitation projections. *Geophysical Research Let-
509 ters*, *45*(19), 10,665–10,672. doi: 10.1029/2018GL079327
- 510 Taylor, K. E., Stouffer, R. J., & Meehl, G. A. (2012). An overview of CMIP5 and
511 the experiment design. *Bulletin of the American Meteorological Society*, *93*(4),
512 485–498. doi: 10.1175/BAMS-D-11-00094.1
- 513 Vose, R. S., Arndt, D., Banzon, V. F., Easterling, D. R., Gleason, B., Huang, B.,
514 . . . Wuertz, D. B. (2012). NOAA’s merged land–ocean surface temperature
515 analysis. *Bulletin of the American Meteorological Society*, *93*(11), 1677–1685.
516 doi: 10.1175/BAMS-D-11-00241.1
- 517 Wehner, M., Gleckler, P., & Lee, J. (2020). Characterization of long period return
518 values of extreme daily temperature and precipitation in the CMIP6 models:
519 Part 1, model evaluation. *Weather and Climate Extremes*, *30*, 100283. doi:
520 10.1016/j.wace.2020.100283
- 521 Wood, R. R., & Ludwig, R. (2020). Analyzing internal variability and forced re-
522 sponse of subdaily and daily extreme precipitation over europe. *Geophysical
523 Research Letters*, *47*(17), e2020GL089300. doi: 10.1029/2020GL089300